LANGMUIR © Cite This: Langmuir 2019, 35, 16583–16592

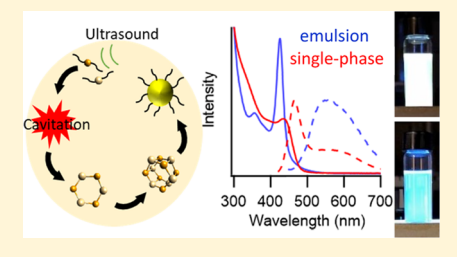
On-Demand Sonochemical Synthesis of Ultrasmall and Magic-Size CdSe Quantum Dots in Single-Phase and Emulsion Systems

Ryan Kastilani, Brittany P. Bishop, Vincent C. Holmberg, and Lilo D. Pozzo*

Department of Chemical Engineering, University of Washington, 3781 Okanogan Lane NE, Seattle, Washington 98195, United

Supporting Information

ABSTRACT: The sonochemical synthesis of CdSe quantum dots (QDs) in a single-liquid bulk phase and in an emulsion-based system is presented. Reactions utilized cadmium oleate and trioctylphosphine selenide precursors and were monitored as a function of sonication time under controlled temperature conditions to isolate the effects of cavitation from those of bulk temperature changes. QD synthesis was found to be slow in the single-phase liquid system (i.e., 1-octadecene) but greatly accelerated in the dispersed system (i.e., emulsions of 1-octadecene in ethylene glycol). It is hypothesized that the emulsion system increases the cavitation efficiency while also delivering acoustic energy in closer proximity to the precursor



molecules. The capacity of CdSe production in the emulsion system was found to be 3.8 g/(L h), which is comparable to the typical hot-injection synthesis of CdSe QDs and can likely be further optimized. While the single-phase solvent system was found to produce ultrasmall QDs that exhibit broadband white-light emission, the emulsion system was found to produce welldefined magic-size clusters (MSCs) with photoluminescence quantum yield as high as 34%. Differences in synthesis rate and product properties from the emulsion and single-phase systems were probed by X-ray diffraction, electron microscopy, UVvisible (vis) and photoluminescence spectroscopy, and small-angle X-ray scattering (SAXS). Finally, precise temporal control of the QD synthesis was demonstrated via on-off cycling of the ultrasound waves.

INTRODUCTION

Over the past decades, there has been great interest in the synthesis and application of semiconductor quantum dots (QDs) due to the fact that they exhibit tunable properties that are drastically different from their bulk counterparts via the effects of quantum confinement. In short, quantum confinement occurs when the characteristic size of a nanoscale particle approaches the exciton Bohr radius of the material, leading to unique optical and electronic properties, which are tunable by the size, shape, and composition of the QD particles. Due to their unique properties, QDs find numerous applications including biolabeling and imaging, light-emitting diodes (LEDs) and phosphors, solar cells, photodetectors, field-effect transistors (FETs), and memory elements.²⁻⁴ A subset of QDs includes magic-size clusters (MSCs), which are small QDs, typically less than 2 nm in diameter, that consist of discrete sizes that correspond to a specific, well-defined number of atoms. 5,6 Their electronic structure sits at the interface between molecules and QDs, and they exhibit unique properties, sharp absorbance features, and entirely surfacestate-based luminescence. Applications and advantages of MSCs include white-light LEDs, facile renal clearance in biological imaging, and their use as starting materials for the generation of more complex nanostructures.

Typically, colloidal QDs are prepared by the hot-injection method, where molecular precursors are injected into a hot solvent at temperatures of up to several hundred degrees celsius, successfully resulting in the synthesis of nanocrystals

(NCs) with variable sizes, shapes, and compositions.^{7,8} Notably, this standard technique has a number of critical drawbacks that make it difficult to scale and that can result in batch-to-batch reproducibility issues. Since the method relies on the rapid injection of up to 50% of the total mixture volume, efficient mixing of the reagents at high temperature becomes difficult as reaction volumes become larger. Likewise, after the initial injection, the reaction temperature often needs to be adjusted quickly to control NC growth, and heat transfer becomes an issue as fluid volume and vessel sizes increase. Alternative approaches include the solvothermal method, where all precursors are initially mixed in a vessel that is then heated and cooled in a controllable manner. However, decoupling of nucleation and growth is necessary to prevent polydispersity, so great care must be taken to ensure that there is sufficient nucleation within a short period of time, otherwise necessitating subsequent size-focusing processes, such as Ostwald ripening, or size-selective post-synthetic purification processes that substantially decrease product yield. Moreover, in the case of multicomponent QDs, it is vital that the mixture be rapidly heated to a temperature where the reactivity of all components is matched, else the composition of the NCs will not reflect that of the original bulk solution.

Received: September 15, 2019 Revised: October 29, 2019 Published: November 21, 2019

16583

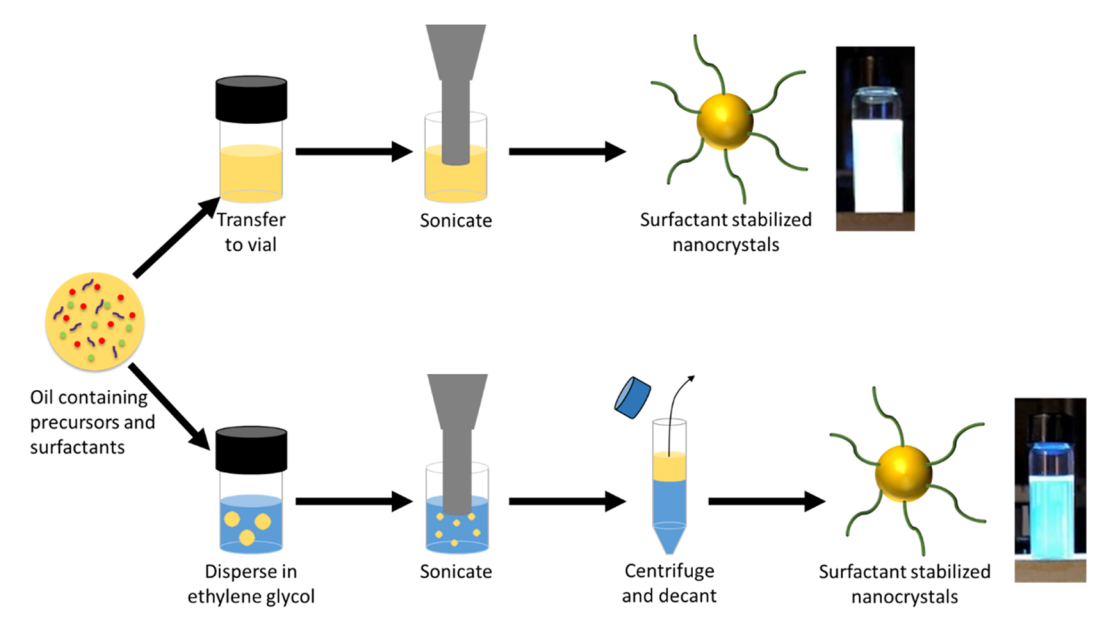


Figure 1. Schematic of the sonochemical nanoparticle synthesis procedure, along with photos of the final products under UV excitation.

A relatively new route toward NC synthesis is through sonochemistry, where ultrasound is applied to a solvent mixture that contains the NC precursors. When ultrasound is applied to a liquid, the alternating positive and negative pressure crests can lead to the formation of transient vapor bubbles or cavities. Furthermore, these bubbles oscillate and grow under repeated compression and expansion cycles, continually gaining potential energy. Eventually, the bubbles grow to a resonant size that can lead to their abrupt and violent collapse, resulting in an extremely rapid release of the accumulated energy in a highly localized space. This results in localized "hotspots" with temperatures that have been estimated to reach 5000 K and pressures in excess of 1000 bar. 10,11 These extreme conditions, albeit spatially and temporally localized, lead to rapid reaction of the precursor molecules, resulting in NC nucleation and growth. Similar sonochemical methods have been used successfully to synthesize a wide variety of dispersed nanomaterials.¹ However, there are few controlled and systematic studies, and the effects of sonication are often convoluted with other effects, including a possible rise of the bulk solvent temperature, which results during continuous sonication without active cooling.

In this work, the sonochemical synthesis of ultrasmall and magic-sized CdSe QDs is reported in single-phase and emulsion-based systems, while actively maintaining the solvent temperature to minimize effects related to bulk temperature increases. We hypothesize that sonochemical synthesis in emulsion systems offers an efficient, accelerated, and controllable pathway toward the on-demand synthesis of complex nanomaterials. A schematic of the synthesis process is shown in Figure 1.

METHODS

Chemicals. 1-Octadecene (90%), oleic acid (90%), oleylamine (70%), cadmium oxide (≥99.99%), selenium (≥99.99%), trioctylphospine (97%) (TOP), and dodecane (≥99%) were purchased from Millipore-Sigma (St. Louis, MO). Hexanes (mixed isomers, 99.9%) and ethylene glycol were purchased from Fisher Scientific (Hampton, NH). All chemicals were used as received.

Precursor Preparation. The cadmium precursor, 84 mM cadmium oleate, is prepared in the following way. To a round-bottom flask, 0.256 g of cadmium oxide, 20 mL of octadecene, and 2.6 mL of oleic acid were added. Using a Schlenk line, the flask is degassed by applying vacuum while stirring at 800 rpm using a magnetic stir bar. Under the nitrogen atmosphere, the flask is heated to 270 °C and is held at this temperature for 30 min or until the mixture becomes clear and colorless; the temperature is then held for 30 additional minutes. At this time, the temperature is lowered to 150 °C, and 1.3 mL of oleylamine is added. The temperature is then lowered to 100 °C, and the flask is degassed for 30 min. Finally, the resulting product is cooled to room temperature. The selenium precursor, 1 M TOP:Se, is prepared by mixing Se powder and TOP overnight in a glovebox until all of the Se is dissolved and the solution is clear and colorless.

Sonochemical Quantum Dot Synthesis. The cadmium precursor is first mixed with the selenium precursor at a 1:4 molar ratio. A schematic of the synthesis process is depicted in Figure 1. In the emulsion system, 2.245 mL of the cadmium precursor is mixed with 0.755 mL of the selenium precursor in a 20 mL glass scintillation vial. The vial is hand-shaken to mix the two precursor solutions, before adding 7 mL of ethylene glycol. The capped vial is again shaken by hand vigorously to create a coarse emulsion. The vial is then placed in a cooling bath containing water at 20 $^{\circ}\text{C}.$ Sonication is then initiated using a Branson 450 Digital Sonifier (400 W max power, 20 kHz), equipped with a 3/8 in. titanium horn directly immersed 0.5 cm into the solution. Sonication is performed continuously at a 20% power setting on the control panel, which has been calibrated to be equivalent to a power dissipation of 12.6 W (See the Supporting Information). Sonication is then temporarily stopped to collect sample aliquots at each relevant time stamp, and an equivalent volume of ethylene glycol is added into the scintillation vial such that the volume is always kept at 10 mL. The volume of aliquot that is withdrawn is such that there is approximately 250 μ L of oil phase (octadecene) in each aliquot. The water in the cooling bath is also exchanged with fresh cold water, and the sonication is continued. The temperature of the vials is also monitored with a thermocouple to separate the effect of sonication/cavitation from that of a possible bulk temperature increase.

Each sample aliquot is then centrifuged and decanted to separate the dispersed oil phase containing the quantum dots from the continuous ethylene glycol phase in the emulsions. These samples are referred to as "unpurified" because of the presence of excess unreacted precursors and organic components. The "as-synthesized" samples are characterized by small-angle X-ray scattering (SAXS) and diluted

about 100-fold in octadecene for UV—visible (vis) spectroscopy as a function of sonication time. For X-ray diffraction (XRD), the assynthesized samples are purified by simply precipitating with the addition of excess ethanol. The powder is then separated and deposited onto a silicon wafer for analysis. Alternatively, the assynthesized samples are diluted 10-fold in dodecane, and purification is performed by liquid—liquid extraction using an equivalent volume of methanol (250 μ L) that is changed three times. After each addition of methanol, the samples are vortexed and centrifuged. Care is taken to replace the dodecane lost during the extraction process to prevent the particles from precipitating since precipitates are not redispersible. After cleaning, particles are also characterized by SAXS, diluted into hexanes 10-fold for UV—vis spectroscopy, 1000-fold for photoluminescence (PL) spectroscopy, and 100-fold for transmission electron microscopy (TEM).

In the single-phase system, the sonication procedure is very similar. The only difference is that the 10 mL reaction volume is entirely composed of the precursor mixture. No ethylene glycol is used and no emulsification is necessary. Also, for these samples, no makeup solvent is added upon removal of sample aliquots as a function of time. The as-synthesized samples are characterized with SAXS and diluted about 10-fold in octadecene for UV-vis spectroscopy. Purification of these samples is also performed by liquid-liquid extraction using an ethanol wash of equivalent volume (250 μ L) three times, after which, the particles spontaneously adhere to the walls of the plastic centrifuge tubes. For XRD sample preparation, the purified samples are redispersed into toluene and drop-cast onto a silicon wafer. Samples are also redispersed into 250 μL of dodecane for characterization in dispersion with SAXS and then diluted into hexanes 10-fold for UVvis spectroscopy, 1000-fold for PL spectroscopy, and 100-fold for TEM.

UV-Visible (UV-Vis) Absorbance and Photoluminescence (PL) Spectroscopy. Both UV-vis and PL spectroscopy are performed using quartz cuvettes with a 1 cm pathlength. UV-vis spectroscopy is performed using a Thermo Scientific Evolution 300 (Waltham, MA) spectrophotometer operating over a 300–700 nm wavelength range. PL spectra are obtained using a Molecular Devices SpectraMax MS (San Jose, CA) fluorescence spectrophotometer. PL quantum yield (PLQY) is measured using an integrating sphere, Hamamatsu C9920, using an excitation wavelength of 360 nm. For PL measurements, the concentration was low enough such that the absorbance at and above 360 nm is below 0.1 to minimize inner-filter effects.

Transmission Electron Microscopy (TEM). Bright-field TEM is performed using FEI Tecnai G2 F20 Super-Twin (Hillsboro, OR) operating at 200 kV. Samples are deposited over a copper TEM grid with 300-mesh carbon from Electron Microscopy Sciences (Hatfield, PA) by drop casting 3 μ L of the sample and letting it dry.

Small-Angle X-ray Scattering (SAXS) and X-ray Diffraction (XRD). SAXS is performed using an Anton-Parr SAXSess (Graz, Austria) Kratky camera in a line-collimation (0.26 Å smearing) configuration with Cu K α radiation. Samples are mounted using 1 mm diameter quartz capillaries. X-ray scattering is collected using a Fujifilm phosphor image plate (Japan) that is then developed in a PerkinElmer Cyclone Plus plate reader (Waltham, MA). The twodimensional (2D) raw data is converted to a one-dimensional (1D) profile and subsequently corrected by subtraction of the scattering from the solvent and from the empty capillary. Absolute scaling of SAXS intensity is performed using a water standard. 12 XRD is performed with a Bruker D8 Discover Microfocus (Billerica, MA) using a beam that has been collimated to a 1 mm cross-section with Cu K α radiation. X-ray diffraction spectra are collected using a Pilatus 3R 100KA 2D detector. The 2D raw data is then converted to a 1D profile and subsequently corrected by subtracting the broad background signal.

■ RESULTS AND DISCUSSION

To determine the total acoustic power that is delivered to the system, calorimetry was performed, as devised by Kikuchi and

Uchida, 13 using water in an insulated environment at the same sonication horn parameters that were used for QD synthesis. Details of the calorimetry experiment are provided in the Supporting Information. Previous sonochemical synthesis of CdSe QDs has shown that particle growth kinetics can be controlled by tuning the ultrasound power; 14 however, it remained unclear if the faster kinetics were due to increased ultrasound cavitation intensity or simply due to the systematic rise in the bulk temperature of the reaction mixture as sonication proceeded. In fact, since no temperature control was implemented in that system, the reaction temperature was observed to rise as high as 200 °C, which is close to the typical temperature used in hot-injection or solvothermal methods for CdSe synthesis. 9,15 In this work, the power delivered by the ultrasound horn was set to 12.6 W for all syntheses. At this power, the reaction temperature stabilizes at a steady state of 55 °C in the single-phase system and 65 °C in the emulsion system. Notably, both of these temperatures are significantly lower than what is typically necessary for either a hot-injection or solvothermal CdSe NC synthesis. Examples of temperature profiles as a function of time are provided in the Supporting Information for each reaction (Figure S1). To ensure that QD formation is due to ultrasound and not due to the mild rise in temperature, a control experiment was performed where the reaction mixture was heated to 60 °C on a hot plate. As would be expected, UV-vis absorbance measurements did not show any changes or QD formation, even after 3 h of heating (Figure S2, Supporting Information).

In our experiments, both the single-phase and emulsion systems were sonicated and tracked for a total of 3 h. Aliquots of the sample were taken at several time points to monitor QD growth as a function of sonication time. Figures 2 and 4 show

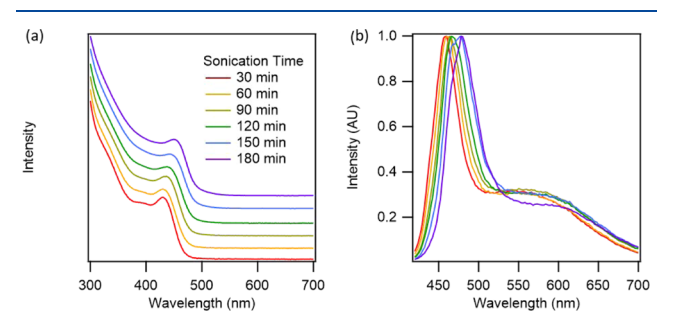


Figure 2. (a) Absorbance and (b) PL spectra ($\lambda_{\rm exc}$ = 360 nm) of CdSe QDs synthesized via sonication in the single-phase solvent system.

UV-vis absorbance and photoluminescence (PL) spectra of the single-phase and emulsion systems, respectively, after purification. UV-vis absorbance spectra were also taken before and after QD purification. Although absorbance and PL spectra carry rich information regarding the QDs, including the clear formation of a 1S_{3/2}1S_e excitonic absorption feature and the associated band-edge luminescence, they also exhibit broad surface-state emission, which can be influenced by a variety of factors including the ligands present on the surface of the QDs. 16-20 To characterize the structure of the QDs, smallangle X-ray scattering (SAXS) was also performed (Figures 3 and 5) as a function of sonication time. In addition, SAXS was also performed before and after sample purification to gain a more complete picture of the changes that occur during the synthesis and purification processes. After each sonochemical synthesis was completed, the samples were also characterized

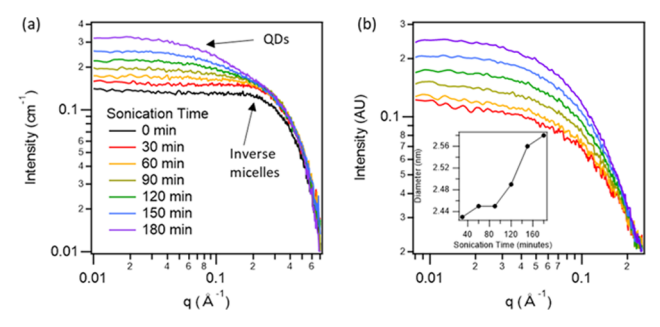


Figure 3. (a) Absolute-scale SAXS profiles of CdSe QDs synthesized via sonication of the single-phase solvent system prior to cleaning and purification. Arrows indicate the two features that correspond to inverse micelles and QDs. (b) Arbitrary-scale SAXS profiles after, with an inset showing the diameter of the QDs extracted from model fitting.

by X-ray diffraction (XRD) and transmission electron microscopy (TEM).

As the precursor mixtures were sonicated in the single-phase and emulsion-based systems, particles were observed to form and steadily grow with longer sonication time. In the singlephase system, the first excitonic peak in the absorbance spectra (Figure 2a) was observed to red-shift along with the band-edge luminescence (Figure 2b) as sonication times increased, indicating gradual growth of the QDs. Using the position of the $1S_{3/2}1S_e$ excitonic absorbance peak,²¹ the QD diameter was estimated as a function of time, growing from a diameter of approximately 1.74 nm after 30 min of sonication to 1.91 nm after 180 min of sonication. In addition to band-edge luminescence, all PL spectra exhibited broad emission at higher wavelengths throughout the visible frequency regime due to the presence of surface states, which are commonly observed for ultrasmall QDs. 22-24 We note that unless the samples are cleaned, the particles will continue to grow very slowly over the course of a month, likely due to secondary phosphine impurities.²⁵ A month after synthesis, the quantum yields of the uncleaned samples are 8%.

SAXS characterization of the particle dispersions further confirms the growth of ultrasmall QDs with increasing time (Figure 3). In SAXS, the scattering intensity profile is related to the square of the Fourier transform of the spatial correlation function of electrons in the sample. The intensity is typically plotted against the scattering wave vector, q, which is dependent on the scattering angle and the X-ray energy or wavelength. Longer spatial correlations appear as features at lower q values, while shorter correlations appear as features at high q. Figure 3a shows the scattering profiles for the single-phase samples as synthesized, prior to cleaning and purification. The data is presented after normalization to an absolute intensity, 12 which allows for direct correlation of SAXS intensity to the concentration of QDs in dispersion.

Notably, prior to the start of the reaction, there is already a scattering profile that arises due to the formation of inverse micelles in the precursor solutions. At longer sonication times, scattering contributions from the CdSe QDs start to dominate the signal. This is especially evident at low q, where a second low-q Guinier "hump" is observed in addition to that found for the precursors prior to sonication. After cleaning the samples, the scattering from the inverse micelles in the precursor is no longer observed, and only a single Guinier turnover is observed at low q (Figure 3b). The scattering

profiles of purified and "cleaned" samples are no longer placed on an absolute scale because there is an inevitable loss of product that is associated with the cleaning process, and the intensities of each profile can no longer be directly compared to one another. Nevertheless, the shape of the scattering profiles only depends on the geometry of the QDs and, under sufficiently dilute conditions, should be independent of the QD concentration. In Figure 3b, the scattering intensities are arbitrarily scaled such that the intensity is matched at high q for qualitative comparison of their shape. As sonication proceeds, the Guinier region shifts toward lower q values, indicating the formation of larger particles. Using the Irena software tool suite, ²⁷ the scattering profiles were fit to a model to extract the QD size. Scattering fits are also provided in the Supporting Information. The mean diameter of the QDs grows from 2.43 nm after 30 min of sonication to 2.58 nm after 180 min of sonication (Figure 3c, inset). The size determined from SAXS is larger when compared to the size calculated from UV-vis absorption features because the head groups of stabilizing ligands that are adsorbed to the surface of the QDs can also contribute to the SAXS signal due to their electron density.

In stark contrast to the above results, when sonochemical QD syntheses are performed in emulsion systems, the results are drastically different. While sonication of the single-phase system produces ultrasmall QDs, sonication of the emulsion-based system produces QDs with well-defined discrete sizes, which are commonly known as magic-sized clusters (MSCs). As the sample is sonicated, no shift of the first excitonic peak is observed in the UV-vis absorbance spectra. Instead, an extremely sharp absorbance peak is observed at 425 nm [full width at half-maximum (fwhm) \approx 100 meV] that does not shift with increasing sonication time but does increase in intensity (Figure 4a). These samples also exhibit broad, "white-

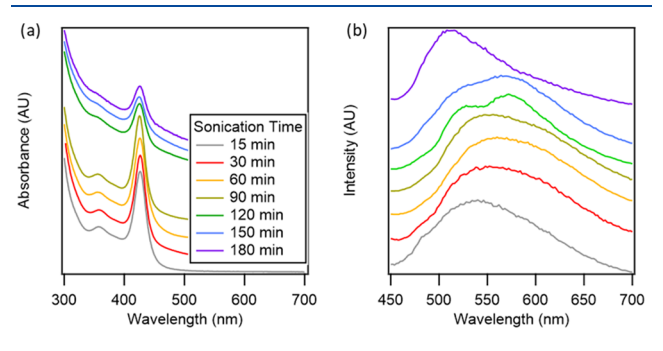


Figure 4. (a) Absorbance and (b) PL spectra ($\lambda_{\rm exc}$ = 420 nm) of cleaned CdSe particles synthesized using sonication in emulsion-based systems as a function of sonication time.

light" emission but with no characteristic band-edge luminescence peak. The photoluminescence excitation (PLE) spectra with emission at 560 nm match the absorbance spectra (Figure S6). Such a sharp absorbance peak coupled with broad surface-state emission but no band-edge luminescence is strongly characteristic of MSCs.^{6,22,28–30} In particular, the absorption peak at this wavelength corresponds well to the known (CdSe)₃₃ and (CdSe)₃₄ MSCs.³¹ Notably, MSCs of (CdSe)₃₃ and (CdSe)₃₄ have very similar size and spectroscopic signatures.^{30–33} Therefore, they are very challenging to isolate and to analyze independently. Since the focus of this work is primarily on the methodology of sonochemical production of CdSe clusters, we did not attempt to isolate

them any further. Interestingly, the relative height of the peak at 425 nm starts to decrease after 90 min of sonication, and an absorption tail starts to appear. This turning point at 120 min is also observed in the PL spectra (Figure 4b). Up until 90 min of sonication, the luminescence is almost entirely characteristic of surface-state emission. However, at ~120 min of sonication, a peak starts to develop that blue-shifts with longer sonication time, bearing resemblance of a band-edge luminescence peak. The formation of a tail in the UV-vis spectra and a peak in the PL spectra suggests that the formation of larger QDs is taking place after extensive sonication. The PL quantum yield (PLQY) after 15 min of sonication is 34%, which is remarkably higher than reported PLQY of CdSe MSCs. 6,28,34-3 Interestingly, the PLQY goes down with longer sonication time (Figure S7), which may be explained by the conversion of MSCs into regular QDs.³⁸ While pinpointing the exact sources of the change in quantum yield would require significant future studies, unshelled CdSe nanocrystals synthesized via hotinjection methods demonstrate similar quantum efficiencies to that of those produced by our reported sonochemical process after long-time sonication or in the single-phase system. Based on the literature, unshelled CdSe nanocrystals produced via hot injection typically exhibit quantum efficiencies ranging from 1 to 30%, 39 which can then be increased up to nearly 100% with carefully engineered shelling processes. 40-Similarly, CdSe MSCs have reported quantum efficiencies that typically range from 0.15 to 22%. ^{6,30,35,43} For example, we carried out a CdSe nanocrystal hot-injection synthesis utilizing cadmium oxide, 1-dodecylphosphonic acid, trioctylphosphine oxide, and hexadecylamine, along with a rapid TOP:Se injection, resulting in ~5 nm diameter nanocrystals with a resultant 6% PLQY (Supporting Information). Notably, this is very close to the PLQY that was achieved after long-time sonication, as the fractional conversion of MSCs to larger nanocrystals increases. Still, while the sonochemical process and hot-injection synthesis methods produce materials with similar photophysical characteristics, the hot-injection method typically necessitates an air-free synthesis system, such as a Schlenk line, where the growth process cannot be turned on and off instantaneously. The sonochemical approach utilizes a technique that is performed at atmospheric conditions, can be scaled readily, and has the added flexibility to turn the growth process on and off on demand. Moreover, the sonication process could also be further optimized to selectively produce or to separate the MSCs as they are synthesized. This would allow for the preservation of the smaller MSCs with their higher PLQY for use in applications that require higher quantum efficiencies.

SAXS was also performed both before and after purification of the emulsion system samples (Figure 5). Similar to the single-phase system, the SAXS data for the emulsion-based system was transformed to an absolute scale for the asprepared samples (Figure 5a). The scattering intensity increases steadily with longer sonication time, indicating that the volume fraction of particles increases with sonication time. The Guinier hump near 0.2 Å⁻¹ is related to the primary particles, viz. CdSe QDs, and the continued rise in intensity toward low q suggests that the particles are associating to create large-scale structures. The intensity continues to rise even at the lowest q values, which means that the size of the aggregates lies beyond the resolution of the SAXS instrument. The samples were subsequently diluted 10-fold, purified, and SAXS was performed again on the cleaned samples in the

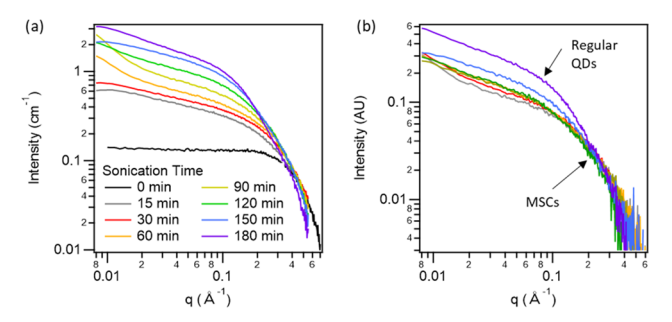


Figure 5. SAXS profiles for CdSe particles synthesized with sonication in an emulsion-based system. (a) As-prepared samples (i.e., before cleaning and purification) in absolute scale units and (b) samples after purification on an arbitrary intensity scale. Arrows indicate the two features that correspond to MSCs and regular QDs.

absence of excess molecular precursors (Figure 5b). Similar to Figure 3a, these SAXS profiles are not placed on an absolute scale since there are some material losses that occur during the purification process. Instead, the scattering profiles were normalized to have matching intensities at high values of q. Even after purification and a 10-fold dilution, the large flocculates continued to persist, as evidenced by the continued rise in intensity at low q. Interestingly, the profiles overlap until 120 min, which matches well with the turning point of the UV-vis spectra, when the intensity of the sharp absorbance feature begins to decrease (Figure 4a). This indicates that the rise in volume fraction with sonication time (Figure 5a) up to 120 min is not due to QD size increases but rather to an increase in the total quantity of MSCs. To further extract structural information, we fit the scattering profiles of the cleaned samples, up to 90 min of sonication, to a model of fractal aggregates of spherical primary particles.⁴⁴ From this model, we obtain a primary particle radius of 7.3 Å that is consistent with the size found by Kasuya et al. for MSCs.³¹ The primary particles then form aggregates with a fractal dimension of 1.3, corresponding to a low-density aggregate. Details of the SAXS models and fits are provided in the Supporting Information. After 120 min, the SAXS profile supports the conclusion that larger QDs are formed, which is most evident in the SAXS profile at 180 min (Figure 5b). The feature at 0.2 Å^{-1} that corresponds to the MSCs is still present, but another feature at 0.1 Å⁻¹ emerges that corresponds to larger QDs.

After 3 h of sonication, samples from both the single-phase and emulsion systems were also purified and characterized by XRD (Figure 6) and TEM (Figure 7). The XRD data exhibits significant peak broadening due to the small size of the QDs produced in both the single-phase and emulsion-based synthesis systems. The XRD profile for the sample from the single-phase system matches that of cubic zincblende CdSe (PDF 04-003-6493, Figure 6a). However, care must be taken because such significant peak broadening cannot decisively differentiate between the cubic zincblende and hexagonal wurtzite structures. ^{6,45,46} The excess signal at low angles is likely due to the remaining ligands in the sample. The diffraction peaks of the material produced from the emulsion system are even broader (Figure 6b) because of the even smaller QD sizes. Notably, MSCs have nearly 80% of their atoms on the surface, which leaves only two unit cells in the core of the particles, ^{22,23} with the observed peaks at 27 and 45°

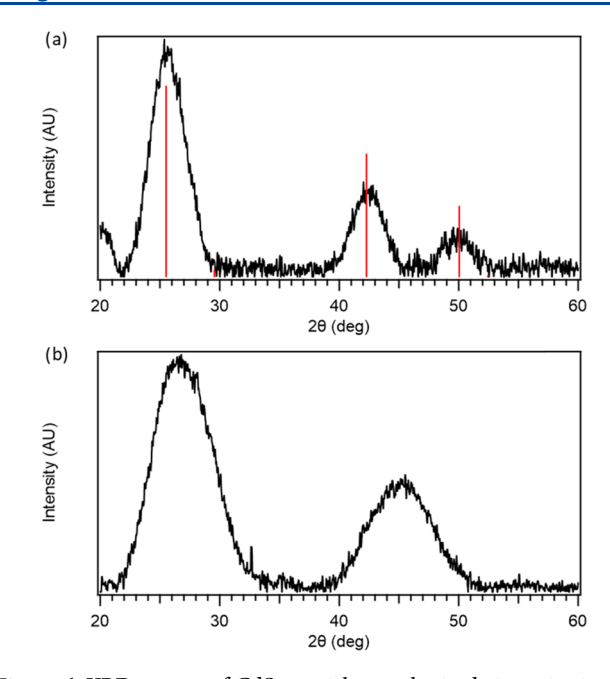


Figure 6. XRD spectra of CdSe particles synthesized via sonication in (a) single-phase and (b) emulsion-based systems. Red lines represent the expected peak positions for the bulk zincblende CdSe structure.

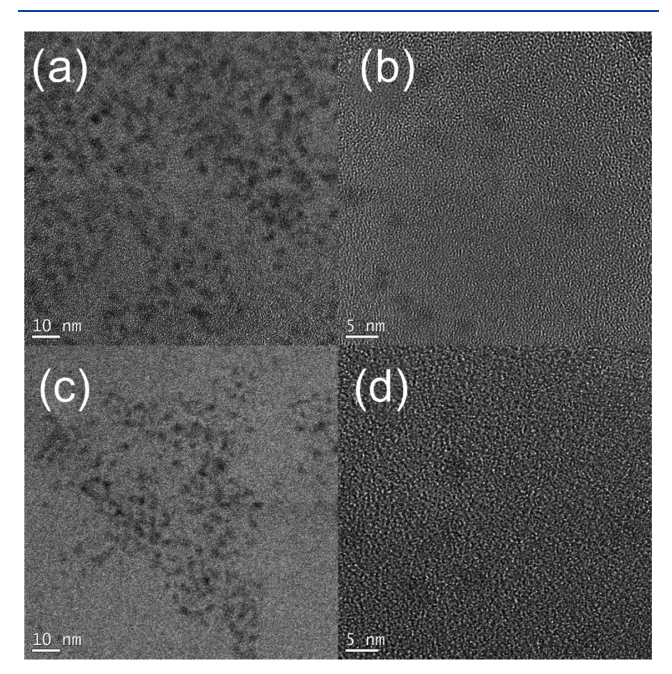


Figure 7. CdSe nanoparticles formed after 180 min of sonication in single phase at (a) low and (b) high magnifications. (c) MSCs formed after 60 min in emulsion-based systems. (d) CdSe nanoparticles formed after 180 min in emulsion-based systems.

corresponding very closely to what has been seen with previous XRD characterization of CdSe and CdS MSCs. 47,48

Figure 7 shows TEM images of the QDs produced via 180 min of sonication in the single-phase system, along with 60 and 180 min of sonication for the emulsion-based system. The contrast in the TEM images is very limited due to the small size of the QDs; nonetheless, the QDs observed from the endpoint of the 3 h emulsion-based synthesis are larger than would be expected for MSCs, which supports the data discussed above that suggested the formation of larger QDs after

extensive sonication. The particles after 180 min of sonication are also larger in size than what was determined from the SAXS profiles after 30 min of sonication and from TEM after 60 min of sonication, further supporting the idea that MSCs are converted into regular-sized QDs after prolonged sonication in emulsions. Given the vanishingly low contrast associated with ultrasmall QDs, it was not possible to obtain high-resolution images of the MSCs using TEM, which is also consistent with the previous literature. ^{30,32,49}

It is important to note that MSCs and ultrasmall QDs are distinct, both in terms of their electronic structure and growth process. While ultrasmall QDs are simply small-sized QDs, MSCs exhibit an electronic structure at the interface between that of a molecule and an inorganic particle, with a specific molecular structure and precisely defined number of atoms that result in a precise electronic excitation that leads to a sharp absorbance peak. Furthermore, since the number of atoms that gives rise to a stable MSC is also precisely defined, MSCs do not grow in a continuous fashion, but rather they transition from one allowed configuration to another. The result is that absorbance peaks do not gradually move or shift, as is the case with regular QDs, but rather they "jump" from one discrete wavelength to another. In this work, the only family of MSCs that was observed corresponds to (CdSe)₃₃ and (CdSe)₃₄. However, it should be noted that numerous other works have successfully synthesized many other families of CdSe MSCs.^{29,50}

Interestingly, in the UV—vis spectra of the samples obtained from the emulsion-based synthesis (Figure 4a), the shrinking of the absorption peak centered at 425 nm is not just relative, but absolute. Prior to purification, the absorbance peak was slightly shifted to 420 nm (Figure S3), likely due to a difference in ligand coordination to the MSC before and after purification. Quantitative tracking of the absorbance at 420 nm with increased sonication time (Figure 8a) shows that the

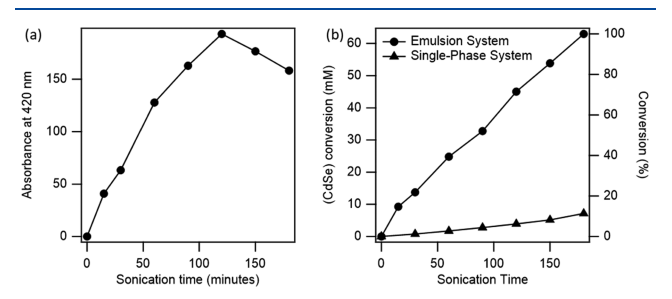


Figure 8. (a) MSC absorbance at 420 nm in the emulsion system tracked as a function sonication time and (b) conversion of Cd and Se precursors into (CdSe) with sonication.

absorbance at 420 nm continues to rise without any shift in wavelength, even after about 120 min of sonication, suggesting that the number of MSCs in the system is increasing as the sample is sonicated. Afterward, however, the absorbance at 420 nm decreases and an absorption tail at longer wavelengths emerges. This coincides with the appearance of a second Guinier region in the SAXS profile after 150 min of sonication (Figure 5b), suggesting that the regular QDs are synthesized at the expense of the MSCs. In other words, the regular QDs are not side products of the sonochemical reaction; instead, QDs are formed from subsequent reactions of MSCs after they are produced. If only MSCs are desired, then the sonication process can be stopped at an appropriate time.

Aside from the difference in product properties, the rate of conversion from precursor to QDs is remarkably faster in the emulsion-based systems. This is evident from the absolutescale SAXS profiles of the samples measured prior to cleaning. Comparing the samples from the single-phase systems (Figure 3a) to the emulsion systems (Figure 5a), the scattering intensity is much higher in the emulsion-based syntheses. In addition, when performing dilutions for UV-vis spectroscopy, the single-phase system samples needed to be diluted 10-fold to get sufficient light penetration through the samples, while the samples from the emulsion systems needed to be diluted more than 100-fold. To further quantify the rate of reaction for the QD and MSC syntheses, the absorption spectra were converted to an energy scale and then integrated from 1.77 to 3.82 eV (325-700 nm). Since the integral of the absorption coefficient over the photon energy (i.e., $\int \alpha dE$) has a negligible size dependence,²¹ the integral of absorbance over energy (i.e., $\int A dE$) can be used to quantify the conversion of Cd and Se precursors into CdSe units across different QD ensembles (Figure 8b). Details and cross-validation of this calculation are given in the Supporting Information. After 3 h of sonication, complete conversion was observed in the emulsion system, while only 11% conversion was observed in the single-phase system. Using a linear fit, the rates of conversion in the emulsion system and in the single-phase system were found to be 3.8 and 0.48 g/(L h), respectively, where the conversion rate of the former is comparable to that of a typical hot-injection synthesis of CdSe ODs. 51,52 For example, an optimized hot-injection synthesis of CdSe QDs yields about 3.7 g/L and it takes approximately 1 h, including the initial heating of the reaction mixture. 53 Thus, sonication in the emulsion system provides a competitive conversion rate for the synthesis of CdSe. Moreover, this rate can likely be further increased by delivering more ultrasound power, using larger volume fractions of oil, increasing precursor concentrations, using a heterogenous selenium source, 55 and/or increasing the reaction temperature.

In addition, when using sonochemical synthesis methods, temporal control over when the reaction starts and stops is remarkable. To demonstrate this, an experiment where the sonication system was systematically turned "on" and "off" every 10 min was also performed with the emulsion-based synthesis. Once again, the absorbance at 420 nm was tracked as a function of elapsed time (Figure 9a). The data clearly shows that the absorbance increases only when the sonication is turned on, which results in a step-like growth curve. When this experiment was repeated with 20 min cycles, the absorbance increased in a similar stepwise manner. Once the absorption data was normalized for the total active sonication time, it was found that the morphology and concentration of the MSCs did not change based on the time interval that was chosen, further supporting that the reactions stop once sonication is removed, with MSC production purely dependent on total active sonication time (Figure S8, Supporting Information). There are several important outcomes from this experiment, which suggest that precise temporal control of the reaction can further elevate QD synthesis methods. First, this conclusively demonstrates that conversion of precursors to QDs is a direct result of ultrasound and not due to a rise in the temperature of the sample, which is a side effect of power dissipation during sonication. Although allowing the temperature to rise may increase QD production rates, such a precise level of temporal control may not be possible and it may also

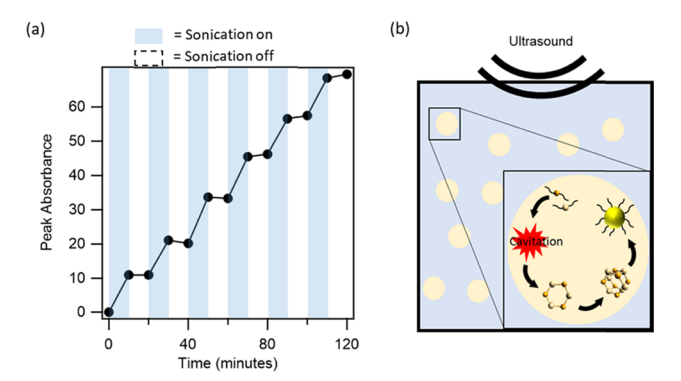


Figure 9. (a) Quantitative absorbance at 420 nm of CdSe MSCs synthesized in the emulsion system with periodic 10 min on—off cycles. Blue shades indicate the time period during which sonication is active. (b) Schematic of the sonochemical QD synthesis mechanism, where cavitation provides the energy required for precursors to react, form clusters, and grow into QDs.

interfere with the selective formation of MSCs observed in the emulsion system. Second, the choice of using trioctylphosphine selenide (TOP:Se) as the chalcogen precursor, as opposed to more reactive secondary phosphine precursors, such as diphenylphosphine selenide, is necessary to carefully control the sonochemical reactions. To note, there are several separate mechanisms for the formation of CdSe monomers. 56 One mechanism requires the decomposition of a tertiary phosphine-chalcogenide to form highly reactive H2Se, while another mechanism does not involve precursor decomposition and instead is a direct reaction of secondary phosphinechalcogenides and metal carboxylates. Since secondary phosphines are much more reactive than tertiary phosphines, 25,57 it has been shown that CdSe MSCs can be synthesized at temperatures as low as 45 °C using diphenylphosphine selenide.²⁸ However, in this application, the low reactivity of TOP:Se prevents unwanted reactions from progressing uncontrollably at low temperatures. The extreme conditions that are locally exhibited by cavitation are more than sufficient to decompose TOP:Se and drive the conversion of CdSe QDs and MSCs. These design choices open the door toward the efficient, on-demand synthesis of QDs, where the reaction can be started and stopped simply by turning the ultrasound on and off. Moreover, secondary phosphines are typically extremely pyrophoric; using TOP:Se allows for the synthesis of QDs without the safety risks associated with such highly reactive precursors. Finally, high-intensity focused ultrasound (HIFU) could also be used to spatially control the synthesis of QDs and MSCs in specific locations.

Two questions remain to be answered: (1) compared to the single-phase system, why is precursor conversion so much faster in the emulsion-based system and (2) why are the resulting products different? The answers to these questions are related. The synthesis of QDs is driven by the extreme conditions induced locally by cavitation. In the single-phase system, bubbles must nucleate homogeneously, which is terribly inefficient. In such cases, cavitation tends to occur predominantly at interfaces such as the vial walls and the surface of the sonication horn. In the emulsion systems, the liquid—liquid interface of the droplets acts as heterogeneous nucleation sites for bubbles, which is much more favorable than homogenous nucleation. ⁵⁸ These "weak spots" in the system have been reasoned previously, ⁵⁹ although no control

experiment in a single-phase bulk system was performed. Moreover, the cavitation bubbles are generated exactly where they are needed, with the sonication energy dissipated locally where the precursor materials are also located (i.e., in the droplets). Hence, sonication of the emulsion system results in more frequent and numerous cavitation events that are more efficiently distributed near the precursors, quickly driving nucleation and growth of the QDs (Figure 9b). This also explains why sonication in the emulsion system results in hotter mixture temperatures than those observed in the single-phase system, even at the same sonication power setting. Coincidentally, the liquid—liquid interface may also serve as a nucleation site for QDs, and it is well known that the energy barrier for heterogenous nucleation is lower than that of homogenous nucleation of QDs.

The high precursor concentration and fast conversion are key to the synthesis of MSCs in the emulsion system. Nevers et al. demonstrated that mixtures with high precursor concentrations offer a well-defined pathway toward synthesizing MSCs, and that the MSCs are stable and resistant toward growth and dissolution.⁶⁰ This is because the MSCs and their ligands form inorganic-organic fibers that, in turn, create ordered mesophases that stabilize the clusters against aggregation. They found that the stability of the MSCs is specifically due to the formation of fibers, rather than the assembled mesophases. In this work, the lack of sharp peaks in the SAXS profiles (Figure 5) suggests that highly ordered mesophases are not created. However, the low fractal dimension of the aggregates ($D_f = 1.3$) does suggest that the MSC aggregates form a nearly linear structure resembling that of a fiber, and this seems sufficient to keep the MSCs stable.

However, instability of the MSCs is evident when samples containing aggregates are diluted, which causes the aggregates to unbundle into individual MSCs. When a diluted sample is left for 36 h at room temperature, the sharp peak at 420 nm is almost completely quenched, and a broad peak emerges (Figure 10a) at lower energies, indicating the formation of

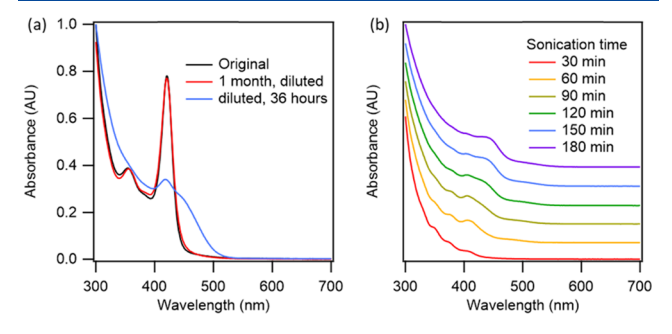


Figure 10. (a) UV—vis absorbance spectra showing the growth and dissolution of MSCs when they do not form large aggregates. (b) UV—vis spectra of as-synthesized samples from the single-phase system collected after different sonication times.

regular QDs. The same phenomenon is observed even with samples that are purified, indicating that these regular QDs are, at least in part, a result of Ostwald ripening. On the other hand, the stability of the MSCs when they are in an aggregated state is remarkable. If a sample is kept in its original higher concentration for a month, its UV—vis spectrum shows no apparent change.

The apparent instability of the MSCs may also explain the decrease in MSC concentration after prolonged sonication in

the emulsion system (Figure 8a). The creation of MSCs is discussed as the result of the extreme temperature and pressure exhibited by cavitation. Cavitation also evokes high-velocity microjets that may dislodge MSCs from their bundles, which could then dissolve or grow into regular QDs. Therefore, there are two competing processes with respect to MSC concentration. Toward the beginning of the sonication process, the system is rich in molecular precursors, and the rate of MSC creation is much faster than the rate of dislodging. Conversely, toward the end of the process, the dislodging of MSCs dominates due to the higher concentration of MSC aggregates and lower concentration of precursors.

In the case of the single-phase reaction system, the resultant ultrasmall QDs may also go through MSC intermediates. Evidence of this can be found in the UV-vis spectra of the assynthesized samples from the single-phase system (Figure 10b). Multiple peaks can clearly be seen, resembling the UVvis spectra of smaller MSCs^{29,61} at earlier sonication times and looking more like the Ostwald ripened MSCs in Figure 10a at longer sonication times. Because the conversion is much slower in the single-phase system, aggregates of MSCs would not be formed because their concentration is low, and hence the MSCs would not be protected from growth and dissolution. Therefore, any MSCs that are formed undergo ripening very quickly, resulting in the regular QDs that are observed in the UV-vis spectra of the purified samples (Figure 2a). This contrasts with the emulsion-based system where the rapid conversion to concentrated MSCs allows for aggregation and stabilization without becoming regular QDs.

CONCLUSIONS

Sonochemical synthesis of CdSe QDs was performed in a single-phase and an emulsion-based system, while keeping the bulk sample temperatures low (<70 °C). Conversion of precursors into QDs is much faster in emulsion systems because the liquid-liquid interfaces serve as heterogeneous nucleation sites for bubbles, which leads to more frequent and more effective cavitation events to drive the reactions. In emulsion systems, MSCs, (CdSe)₃₃, and (CdSe)₃₄ were synthesized, although prolonged sonication beyond 120 min does also lead to the formation of regular QDs. In addition to ligand-based stabilization, the MSCs are stabilized via the formation of extended inorganic-organic aggregates, which are enabled by the rapid rise in MSC concentration in the emulsion-based system. Unbundling of these aggregates by dilution destabilizes the MSCs, resulting in dissolution and growth of MSCs into regular QDs. In the single-phase bulk synthesis systems, evidence suggests that MSCs are created as intermediates to QD synthesis; however, because the reaction rate is slow, the MSC concentration is too low to form stable aggregates, and instead, they undergo Ostwald ripening to form regular QDs. Controlled, on-demand synthesis of CdSe QDs is also demonstrated by simply turning the ultrasound on and off at any arbitrary rate. The rate of QD production in the emulsion system was found to be 3.8 g/(L h) with complete conversion of precursors, which is much faster than that in the single-phase system [0.48 g/(L h)] and is comparable to that of the typical hot-injection QD synthesis, and can likely be further optimized. Letting the temperature rise higher may speed up QD production but likely at the cost of a loss in temporal reaction control. Finally, although this work focuses on CdSe QDs, there are no theoretical limitations that would prevent the synthesis of other types of QDs. Future work will

involve a more detailed characterization of these CdSe QDs, along with other types of semiconductor materials.

ASSOCIATED CONTENT

S Supporting Information

The Supporting Information is available free of charge at https://pubs.acs.org/doi/10.1021/acs.langmuir.9b02891.

Temperature profile of the reaction mixture, control sample using a hot plate, as-synthesized UV—vis spectra of samples from the emulsion system, SAXS data fitting, CdSe conversion calculation, absorbance normalization by active sonication time, and hot-injection synthesis of CdSe nanocrystals (PDF)

AUTHOR INFORMATION

Corresponding Author

*E-mail: dpozzo@u.washington.edu.

ORCID ®

Vincent C. Holmberg: 0000-0002-9591-8951

Lilo D. Pozzo: 0000-0001-7104-9061

Notes

The authors declare no competing financial interest.

ACKNOWLEDGMENTS

Acknowledgment is made to the National Science Foundation (NSF) through the UW Molecular Engineering Materials Center, a Materials Research Science and Engineering Center (DMR-1719797) for support of this research. L.D.P. also acknowledges the Donors of the American Chemical Society Petroleum Research Fund. We also acknowledge Prof. Brandi Cossairt from the Department of Chemistry at the University of Washington for her expert input into this project. Part of this work was conducted at the Molecular Analysis Facility, a National Nanotechnology Coordinated Infrastructure site at the University of Washington, which is supported in part by the National Science Foundation (grant ECC-1542101), the University of Washington, the Molecular Engineering & Sciences Institute, the Clean Energy Institute, and the National Institutes of Health. This research made use of a laboratory SAXS instrument at the UW that is funded by the National Science Foundation under grant No. DMR-0817622. This work benefited from the use of the SasView application, originally developed under NSF award DMR-0520547. Sas-View contains code developed with funding from the European Union's Horizon 2020 research and innovation programme under the SINE2020 project, grant agreement No 654000.

REFERENCES

- (1) Bawendi, M. G.; Steigerwald, M. L.; Brus, L. E. The Quantum Mechanics of Larger Semiconductor Clusters ("Quantum Dots"). *Annu. Rev. Phys. Chem.* **1990**, *41*, 477–496.
- (2) Michaleí, X.; Pinaud, F. F.; Bentolila, L. A.; Tsay, J. M.; Doose, S.; Li, J. J.; Sundaresan, G.; Wu, A. M.; Gambhir, S. S.; Weiss, S. Quantum Dots for Live Cells, in Vivo Imaging, and Diagnostics. *Science* **2005**, 307, 538–544.
- (3) Shen, W.; Tang, H.; Yang, X.; Cao, Z.; Cheng, T.; Wang, X.; Tan, Z.; You, J.; Deng, Z. Synthesis of Highly Fluorescent InP/ZnS Small-Core/Thick-Shell Tetrahedral-Shaped Quantum Dots for Blue Light-Emitting Diodes. *J. Mater. Chem. C* **2017**, *5*, 8243–8249.
- (4) Talapin, D. V.; Lee, J.; Kovalenko, M. V.; Shevchenko, E. V. Prospects of Colloidal Nanocrystals for Electronic and Optoelectronic Applications. *Chem. Rev.* **2010**, *110*, 389–458.

- (5) Yu, Q.; Liu, C. Y. Study of Magic-Size-Cluster Mediated Formation of Cds Nanocrystals: Properties of the Magic-Size Clusters and Mechanism Implication. *J. Phys. Chem. C* **2009**, *113*, 12766–12771
- (6) Harrell, S. M.; McBride, J. R.; Rosenthal, S. J. Synthesis of Ultrasmall and Magic-Sized CdSe Nanocrystals. *Chem. Mater.* **2013**, 25, 1199–1210.
- (7) Rao, C. N. R.; Vivekchand, S. R. C.; Biswas, K.; Govindaraj, A. Synthesis of Inorganic Nanomaterials. *Dalton Trans.* **2006**, 3728–3749.
- (8) Park, J.; Joo, J.; Soon, G. K.; Jang, Y.; Hyeon, T. Synthesis of Monodisperse Spherical Nanocrystals. *Angew. Chem., Int. Ed.* **2007**, 46, 4630–4660.
- (9) Van Embden, J.; Chesman, A. S. R.; Jasieniak, J. J. The Heat-up Synthesis of Colloidal Nanocrystals. *Chem. Mater.* **2015**, *27*, 2246–2285.
- (10) Suslick, K. S. Sonochemistry. Science 1990, 247, 1439-1445.
- (11) Bang, J. H.; Suslick, K. S. Applications of Ultrasound to the Synthesis of Nanostructured Materials. *Adv. Mater.* **2010**, 22, 1039–1059.
- (12) Fan, L.; Degen, M.; Bendle, S.; Grupido, N.; Ilavsky, J. The Absolute Calibration of a Small-Angle Scattering Instrument with a Laboratory X-Ray Source. *J. Phys.: Conf. Ser.* **2010**, 247, No. 012005.
- (13) Kikuchi, T.; Uchida, T. Calorimetric Method for Measuring High Ultrasonic Power Using Water as a Heating Material. *J. Phys.: Conf. Ser.* **2011**, 279, No. 012012.
- (14) Murcia, M. J.; Shaw, D. L.; Woodruff, H.; Naumann, C. A.; Young, B. A.; Long, E. C. Facile Sonochemical Synthesis of Highly Luminescent ZnS-Shelled CdSe Quantum Dots. *Chem. Mater.* **2006**, *18*, 2219–2225.
- (15) Kim, J. Y.; Voznyy, O.; Zhitomirsky, D.; Sargent, E. H. 25th Anniversary Article: Colloidal Quantum Dot Materials and Devices: A Quarter-Century of Advances. *Adv. Mater.* 2013, 25, 4986–5010.
- (16) Majetich, S. A.; Carter, A. C. Surface Effects on the Optical Properties of Cadmium Selenide Quantum Dots. *J. Phys. Chem. A.* **1993**, 97, 8727–8731.
- (17) Ning, Z.; Molnár, M.; Chen, Y.; Friberg, P.; Gan, L.; Ågren, H.; Fu, Y. Role of Surface Ligands in Optical Properties of Colloidal CdSe/CdS Quantum Dots. *Phys. Chem. Chem. Phys.* **2011**, *13*, 5848–5854
- (18) Leatherdale, C. A.; Woo, W. K.; Mikulec, F. V.; Bawendi, M. G. On the Absorption Cross Section of CdSe Nanocrystal Quantum Dots. *J. Phys. Chem. B* **2002**, *106*, 7619–7622.
- (19) Lazarenkova, O. L.; Balandin, A. A. Electron and Phonon Energy Spectra in a Three-Dimensional Regimented Quantum Dot Superlattice. *Phys. Rev. B* **2002**, *66*, No. 245319.
- (20) Jiang, C.-W.; Green, M. A. Silicon Quantum Dot Superlattices: Modeling of Energy Bands, Densities of States, and Mobilities for Silicon Tandem Solar Cell Applications. *J. Appl. Phys.* **2006**, 99, No. 114902.
- (21) Jasieniak, J.; Smith, L.; Van Embden, J.; Mulvaney, P.; Califano, M. Re-Examination of the Size-Dependent Absorption Properties of CdSe Quantum Dots. *J. Phys. Chem. C* **2009**, *113*, 19468–19474.
- (22) Landes, C. F.; Braun, M.; El-Sayed, M. A. On the Nanoparticle to Molecular Size Transition: Fluorescence Quenching Studies. *J. Phys. Chem. B* **2001**, *105*, 10554–10558.
- (23) McBride, J. R.; Dukes, A. D.; Schreuder, M. A.; Rosenthal, S. J. On Ultrasmall Nanocrystals. *Chem. Phys. Lett.* **2010**, 498, 1–9.
- (24) Bowers, M. J.; McBride, J. R.; Rosenthal, S. J. White-Light Emission from Magic-Sized Cadmium Selenide Nanocrystals. *J. Am. Chem. Soc.* **2005**, 127, 15378–15379.
- (25) Evans, C. M.; Evans, M. E.; Krauss, T. D. Mysteries of TOPSe Revealed: Insights into Quantum Dot Nucleation. *J. Am. Chem. Soc.* **2010**, *132*, 10973–10975.
- (26) De La Iglesia, P.; Jaeger, V. W.; Xi, Y.; Pfaendtner, J.; Pozzo, L. D. Structure Characterization and Properties of Metal-Surfactant Complexes Dispersed in Organic Solvents. *Langmuir* **2015**, *31*, 9006–9016.

(27) Ilavsky, J.; Jemian, P. R. Irena: Tool Suite for Modeling and Analysis of Small-Angle Scattering. *J. Appl. Crystallogr.* **2009**, 42, 347–353.

- (28) Cossairt, B. M.; Owen, J. S. CdSe Clusters: At the Interface of Small Molecules and Quantum Dots. *Chem. Mater.* **2011**, 23, 3114–3119.
- (29) Kudera, S.; Zanella, M.; Giannini, C.; Rizzo, A.; Li, Y.; Gigli, G.; Cingolani, R.; Ciccarella, G.; Spahl, W.; Parak, W. J.; et al. Sequential Growth of Magic-Size CdSe Nanocrystals. *Adv. Mater.* **2007**, *19*, 548–552.
- (30) Dukes, A. D.; McBride, J. R.; Rosenthal, S. J. Synthesis of Magic-Sized CdSe and CdTe Nanocrystals with Diisooctylphosphinic Acid. *Chem. Mater.* **2010**, *22*, 6402–6408.
- (31) Kasuya, A.; Sivamohan, R.; Barnakov, Y. A.; Dmitruk, I. M.; Nirasawa, T.; Romanyuk, V. R.; Kumar, V.; Mamykin, S. V.; Tohji, K.; Jeyadevan, B.; et al. Ultra-Stable Nanoparticles of CdSe Revealed from Mass Spectrometry. *Nat. Mater.* **2004**, *3*, 99–102.
- (32) Jadhav, A. A.; More, P. V.; Khanna, P. K. Rapid Microwave Synthesis of White Light Emitting Magic Sized Nano Clusters of CdSe: Role of Oleic Acid. *RSC Adv.* **2015**, *5*, 76733–76742.
- (33) Wang, Y.; Zhang, Y.; Wang, F.; Giblin, D. E.; Hoy, J.; Rohrs, H. W.; Loomis, R. A.; Buhro, W. E. The Magic-Size Nanocluster (CdSe)₃₄ as a Low-Temperature Nucleant for Cadmium Selenide Nanocrystals; Room-Temperature Growth of Crystalline Quantum Platelets. *Chem. Mater.* **2014**, *26*, 2233–2243.
- (34) Cossairt, B. M.; Juhas, P.; Billinge, S. J. L.; Owen, J. S. Tuning the Surface Structure and Optical Properties of CdSe Clusters Using Coordination Chemistry. *J. Phys. Chem. Lett.* **2011**, *2*, 3075–3080.
- (35) Sadeghi, S.; Khabbaz Abkenar, S.; Ow-Yang, C. W.; Nizamoglu, S. Efficient White LEDs Using Liquid-State Magic-Sized CdSe Quantum Dots. *Sci. Rep.* **2019**, *9*, No. 10061.
- (36) Liu, X.; Jiang, Y.; Wang, C.; Li, S.; Lan, X.; Chen, Y. White-Light-Emitting CdSe Quantum Dots with "Magic Size" via One-Pot Synthesis Approach. *Phys. Status Solidi A* **2010**, 207, 2472–2477.
- (37) Dolai, S.; Dutta, P.; Muhoberac, B. B.; Irving, C. D.; Sardar, R. Mechanistic Study of the Formation of Bright White Light-Emitting Ultrasmall CdSe Nanocrystals: Role of Phosphine Free Selenium Precursors. *Chem. Mater.* **2015**, *27*, 1057–1070.
- (38) Dai, S.; Su, Y. S.; Chung, S. R.; Wang, K. W.; Pan, X. Controlling the Magic Size of White Light-Emitting CdSe Quantum Dots. *Nanoscale* **2018**, *10*, 10256–10261.
- (39) Qu, L.; Peng, A.; Peng, X. Alternative Routes toward High Quality CdSe Nanocrystals. *Nano Lett.* **2001**, *1*, 333–337.
- (40) Chen, O.; Zhao, J.; Chauhan, V. P.; Cui, J.; Wong, C.; Harris, D. K.; Wei, H.; Han, H.; Fukumura, D.; Jain, R. K.; Bawendi, M. G. Compact High-quality CdSe-CdS core-shell nanocrystals with narrow emission linewidths and suppressed blinking. *Nat. Mater.* **2013**, *12*, 445–451.
- (41) Jeong, B. Y.; Park, Y.; Chang, J. H.; Cho, I.; Kim, J. K.; Kim, H.; Char, K.; Cho, J.; Klimov, V. I.; Park, P.; Lee, D. C.; Bae, W. K. Colloidal Spherical Quantum Wells with Near-Unity Photoluminescence Quantum Yield and Suppressed Blinking. *ACS Nano* **2016**, *10*, 9297–9305.
- (42) Christodoulou, S.; Vaccaro, G.; Pinchetti, V.; De Donato, F.; Grim, J. Q.; Casu, A.; Genovese, A.; Vicidomini, G.; Diaspro, A.; Brovelli, S.; Manna, L.; Moreels, I. Synthesis of Highly Luminescent Wurtzite CdSe/CdS Giant-Shell Nanocrystals Using a Fast Continuous Injection Route. *J. Mater. Chem. C* 2014, 2, 3439–3447.
- (43) Lysova, I.; Anton, H.; Dmitruk, I.; Mely, Y. Tuning Luminescent Properties of CdSe Nanoclusters by Phosphine Surface Passivation. *Methods Appl. Fluoresc.* **2016**, *4*, No. 044009.
- (44) Teixeira, J. Small-Angle Scattering by Fractal Systems. *J. Appl. Crystallogr.* **1988**, *21*, 781–785.
- (45) Talapin, D. V.; Rogach, A. L.; Kornowski, A.; Haase, M.; Weller, H. Highly Luminescent Monodisperse CdSe and CdSe/ZnS Nanocrystals Synthesized in a Hexadecylamine-Trioctylphosphine Oxide-Trioctylphospine Mixture. *Nano Lett.* **2001**, *1*, 207–211.

- (46) Kodama, K.; Iikubo, S.; Taguchi, T.; Shamoto, S. I. Finite Size Effects of Nanoparticles on the Atomic Pair Distribution Functions. *Acta Crystallogr., Sect. A: Found. Crystallogr.* **2006**, *62*, 444–453.
- (47) Xia, Y.-S.; Zhu, C.-Q. Aqueous Synthesis of Luminescent Magic Sized CdSe Nanoclusters. *Mater. Lett.* **2008**, *62*, 2103–2105.
- (48) Williamson, C. B.; Nevers, D. R.; Nelson, A.; Hadar, I.; Banin, U.; Hanrath, T.; Robinson, R. D. Chemically Reversible Isomerization of Inorganic Clusters. *Science* **2019**, *363*, 731–735.
- (49) Gary, D. C.; Terban, M. W.; Billinge, S. J. L.; Cossairt, B. M. Two-Step Nucleation and Growth of InP Quantum Dots via Magic-Sized Cluster Intermediates. *Chem. Mater.* **2015**, *27*, 1432–1441.
- (50) Ouyang, J.; Zaman, M. B.; Yan, F. J.; Johnston, D.; Li, G.; Wu, X.; Leek, D.; Ratcliffe, C. I.; Ripmeester, J. A.; Yu, K. Multiple Families of Magic-Sized CdSe Nanocrystals with Strong Bandgap Photoluminescence via Noninjection One-Pot Syntheses. *J. Phys. Chem. C* 2008, 112, 13805–13811.
- (51) Abe, S.; Čapek, R. K.; De Geyter, B.; Hens, Z. Tuning the Postfocused Size of Colloidal Nanocrystals by the Reaction Rate: From Theory to Application. *ACS Nano* **2012**, *6*, 42–53.
- (52) Jasieniak, J.; Bullen, C.; Van Embden, J.; Mulvaney, P. Phosphine-Free Synthesis of CdSe Nanocrystals. *J. Phys. Chem. B* **2005**, *109*, 20665–20668.
- (53) Protière, M.; Nerambourg, N.; Renard, O.; Reiss, P. Rational Design of the Gram-Scale Synthesis of Nearly Monodisperse Semiconductor Nanocrystals. *Nanoscale Res. Lett.* **2011**, *6*, No. 472.
- (54) Williamson, C. B.; Nevers, D. R.; Hanrath, T.; Robinson, R. D. Prodigious Effects of Concentration Intensification on Nanoparticle Synthesis: A High-Quality, Scalable Approach. *J. Am. Chem. Soc.* **2015**, *137*, 15843–15851.
- (55) Flamee, S.; Cirillo, M.; Abe, S.; De Nolf, K.; Gomes, R.; Aubert, T.; Hens, Z. Fast, High Yield, and High Solid Loading Synthesis of Metal Selenide Nanocrystals. *Chem. Mater.* **2013**, 25, 2476–2483.
- (56) Frenette, L. C.; Krauss, T. D. Uncovering Active Precursors in Colloidal Quantum Dot Synthesis. *Nat. Commun.* **2017**, *8*, No. 2082.
- (57) Ruberu, T. P. A.; Albright, H. R.; Callis, B.; Ward, B.; Cisneros, J.; Fan, H.-J.; Vela, J. Molecular Control of the Nanoscale: Effect of Phosphine-Chalcogenide Reactivity on CdS-CdSe Nanocrystal Composition and Morphology. ACS Nano 2012, 6, 5348–5359.
- (58) Brennen, C. E. Cavitation and Bubble Dynamics, 1st ed.; Cambridge University Press: Cambridge, 2013.
- (59) Sivakumar, M.; Towata, A.; Yasui, K.; Tuziuti, T.; Kozuka, T.; Iida, Y.; Maiorov, M. M.; Blums, E.; Bhattacharya, D.; Sivakumar, N.; et al. Ultrasonic Cavitation Induced Water in Vegetable Oil Emulsion Droplets A Simple and Easy Technique to Synthesize Manganese Zinc Ferrite Nanocrystals with Improved Magnetization. *Ultrason. Sonochem.* 2012, 19, 652–658.
- (60) Nevers, D. R.; Williamson, C. B.; Savitzky, B. H.; Hadar, I.; Banin, U.; Kourkoutis, L. F.; Hanrath, T.; Robinson, R. D. Mesophase Formation Stabilizes High-Purity Magic-Sized Clusters. *J. Am. Chem. Soc.* 2018, 140, 3652–3662.
- (61) Beecher, A. N.; Yang, X.; Palmer, J. H.; Lagrassa, A. L.; Juhas, P.; Billinge, S. J. L.; Owen, J. S. Atomic Structures and Gram Scale Synthesis of Three Tetrahedral Quantum Dots. *J. Am. Chem. Soc.* **2014**, *136*, 10645–10653.